Surface diffusion of Au on Si(111): A microscopic study

J. Slezák,* M. Ondřejček, Z. Chvoj, and V. Cháb
Institute of Physics, Academy of Sciences of the Czech Republic, Cukrovarnická 10, 162 53 Prague, Czech Republic

H. Conrad
Fritz-Haber Institut, Faradayweg 4-6, D-14195 Berlin, Germany

S. Heun, Th. Schmidt, B. Ressel, and K. C. Prince
Sincrotrone Trieste, Basovizza, I-34012 Trieste, Italy
(Received 15 November 1999)

The direct evolution of submonolayer two-dimensional Au phases on the Si(111)-(7×7) surface was studied in real time using the spectroscopic photoemission and low energy electron microscope located at the synchrotron radiation source ELETTRA. A finite area covered by 1 monolayer (ML) of gold with a steplike transition zone was prepared by evaporation *in situ*. Subsequent annealing resulted in the spread of the Au layer and the formation of laterally extended Si(111)-(5×1)-Au and Si(111)-($\sqrt{3}\times\sqrt{3}$)$R30°$-Au surface reconstructions. At a temperature around 970 K, the boundary of the gold-covered region propagates on the clean Si(111)-(7×7) and exhibits a nonlinear dependence on time. The ordered Si(111)-(5×1)-Au plateau develops a separated front moving with constant velocity. Two values of the Au diffusion coefficients were estimated at a temperature of about 985 K: (1) $D_{7\times7}=5.2\times10^{-8}$ cm^2 s^{-1} as the average diffusion coefficient for Au on a clean Si(111)-(7×7) surface in the concentration range from 0.4 ML up to 0.66 ML and (2) $D_{5\times1}=1.2\times10^{-7}$ cm^2 s^{-1} as the lower limit for the diffusion of single Au atoms on the Si(111)-(5×1)-Au ordered phase.

I. INTRODUCTION

Experimental investigations of surface diffusion represent an important field of surface physics since they can provide detailed information on both kinetics and dynamics in adsorbed layers. The major factor that makes surface diffusion complex and interesting from a scientific point of view is the interaction between diffusing particles (direct or indirect via the substrate), as a result of which a diffusing region may self-organize. It has been confirmed experimentally in Refs. 1–4 that in the course of diffusion an adsorbate may form surprisingly long-distance ordered phases on the surface. For instance, the observation of plateau-like parts in the concentration profile is usually correlated with the appearance of phase transitions at particular coverages, which in turn leads to local maximum or minimum values of the diffusion coefficient.[1,5] However, the connection between the plateau-like parts in the diffusion front and the evolution of ordered phases has not been directly demonstrated up to now, mainly due to the use of methods lacking structural information or imaging techniques with insufficient lateral resolution [for example, the photoemission electron microscopy using a mercury short-arc lamp (PEEM) resolution in Refs. 1 and 2 is ≈10 μm]. In particular, the diffusion properties of metals on semiconductor surfaces and interfaces have drawn much attention from industrial researchers since phenomena such as electromigration and diffusion[6,7] may restrict the use of electronic microstructures.

Si(111) is a prototypical surface, and shows a rich variety of surface reconstructions upon metal adsorption. For Au on Si(111), different surface reconstructions have been identified at various elevated temperatures:[8,9] Si(111)-(5×1)-Au, Si(111)-($\sqrt{3}\times\sqrt{3}$)$R30°$-Au, Si(111)-(6×6)-Au, and the high temperature phase Si(111)-(1×1)-Au. The first structure, also denoted as (5×2)-Au in the literature, appears during the initial stages of Au adsorption on a Si(111)-(7×7) surface at substrate temperatures above 620 K.[10] The saturation coverage of (5×1)-Au has been estimated to be 0.443 monolayer (ML) [1 ML=one Au atom per surface Si atom on the ideal unreconstructed Si(111) face $=7.84\times10^{14}$ atoms/cm^2]. For the gold-rich ($\sqrt{3}\times\sqrt{3}$)$R30°$-Au structure (denoted $\sqrt{3}$ -Au in the following) a coverage of 0.665 ML has been reported.[8,9] Further deposition after the completion of the $\sqrt{3}$-Au structure leads to the appearance of three-dimensional Au particles, which grow and occasionally coalesce. The disordered Si(111)-(6×6)-Au structure, which exhibits a ($\sqrt{3}\times\sqrt{3}$)$R30°$ low-energy electron diffraction (LEED) pattern with diffuse rings [known as β-$\sqrt{3}$ (Ref. 11)], is observed at a gold coverage of 1 ML. Gold deposition at room temperature on a clean Si(7×7) surface makes the LEED pattern fade away, and only after deposition of large amounts of gold do spots due to three-dimensional metal islands appear.

Structural models for the reconstructions listed above have been proposed[9,10] on the basis of scanning tunneling microscopy (STM) studies but a general consensus has yet to be achieved. According to the current models, both the (5×1)-Au and $\sqrt{3}$-Au appear to have gold contents that depend strongly on temperature. At higher temperatures gold atoms might diffuse into the bulk and/or partially desorb.

The aim of this work is to present a consistent, semiquantitative picture of Au/Si(111) surface diffusion at submonolayer coverages. The application of spectroscopic photoemis-

sion and low energy electron microscope[12] (SPELEEM) as a local spectroscopic probe enabled us to measure directly the local gold concentration and the time evolution of two different gold surface phases directly with good spatial and temporal resolution. The diffusion coefficients for Au diffusion at elevated stages were estimated.

II. EXPERIMENT

The experiments were performed[12] with the multipurpose SPELEEM located at the ELETTRA synchrotron radiation source in Trieste, Italy. The instrument can be used alternately for PEEM, soft-x-ray photoemission electron microscopy using synchrotron radiation (XPEEM), low energy electron microscopy (LEEM), LEED, mirror electron microscopy (MEM), and other imaging modes depending on the particular problem studied.

In the investigations that are reported here, the sample preparation was as follows: *p*-type silicon wafers were cut to 1×1 cm^2 squares and mounted on a sample cartridge with a Mo cap. Heating was achieved by electron bombardment of the Si wafer from the back. The initial *in situ* cleaning consisted of short flashes up to 1500 K after outgassing at lower temperatures, usually overnight. In the SPELEEM preparation chamber, gold was deposited from a UHV evaporator (EFM3 Focus, Omicron Ltd.) with a tungsten spiral supporting a gold droplet. The evaporation rate was calibrated with LEEM and LEED beforehand: since the completion of the (5×1)-Au and $\sqrt{3}$-Au structures is clearly visible in LEEM, an evaporation time was measured for these known coverages, and the deposition time needed for 1 ML was determined. 1 ML was typically completed after 9 min with the sample temperature kept at 750 K during evaporation. A movable shutter was positioned about 1 mm above the sample plane, and during evaporation it was touching the cap of the cartridge (not the sample) to eliminate mechanical vibrations. It enabled one half of the sample to be covered with a gold layer. During the Au evaporation the pressure rose to 4×10^{-7} Pa. The base pressure did not exceed 1×10^{-7} Pa during the diffusion experiments at high temperature.

The sample temperature was measured with a W-Re thermocouple spot-welded to a small tantalum plate touching the Si sample. The precision in temperature reading was estimated to be ±50 K. The thermocouple was calibrated in preliminary experiments using the $(7\times7)\Leftrightarrow(1\times1)$ phase transition of the clean Si(111) surface at 1120 K.[13] Data were recorded with a slow-scan charge-coupled device (CCD) camera or with a video camera. The background modulation at fixed position in the images, such as the inhomogeneous intensity distribution and a few spots, is due to the spatially varying electron yield of the channel plates. The video images were digitized at the Fritz-Haber Institute in Berlin.

III. RESULTS

The initial state for the surface diffusion measurements was prepared by covering about half of the substrate at 750 K with a 1 ML Au layer, as described in the preceding section. The resulting border area is shown as a PEEM image in Fig. 1(a). Since the brightness directly reflects the work function distribution, the uncovered Si(111)-(7×7) region appears brighter than the gold-covered parts in agreement with a recent study[14] in which an increasing work function with Au coverage up to about 0.5 ML was observed. The circular brightness modulation and the dark spot at the center of the screen are artefacts due to the inhomogeneity of the channel plate mentioned above. In order to obtain a quantitative measure of the concentration across the border we determined an intensity profile along the oblong region from *A* to *B* marked in Fig. 1(a), averaged over the shorter side of the rectangle. The transition zone [Fig. 1(b)] exhibits a concentration increase over ≈10 μm. This shape is explained by a penumbra effect due to the evaporation geometry and implies that the gold atoms stay at the impact position. As the sample temperature during evaporation was clearly above the formation

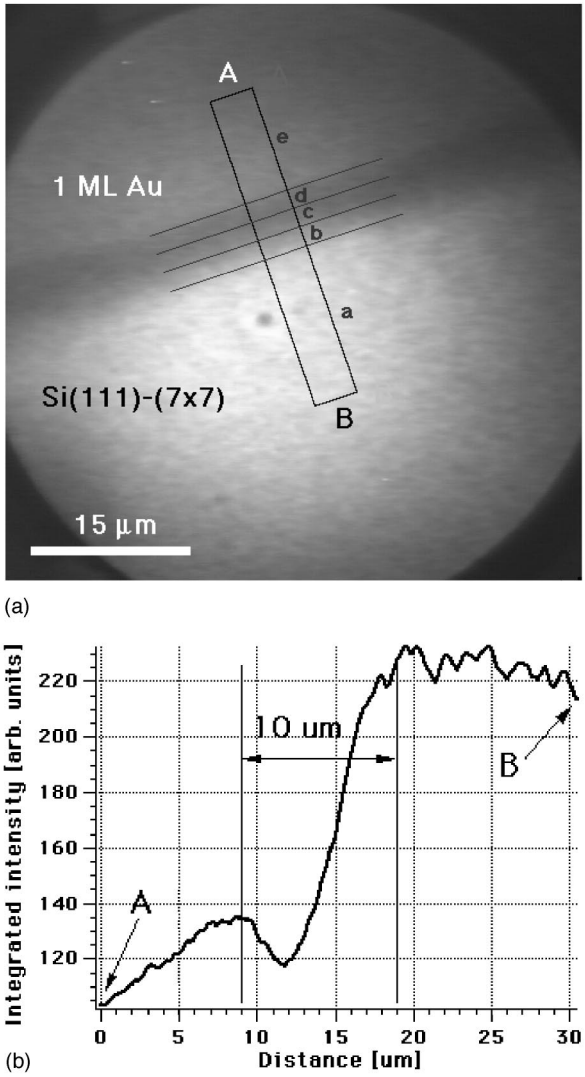

FIG. 1. (a) A PEEM image of the profile taken immediately after Au deposition at 750 K. Integrated cross-sectional intensity [see (b)] was acquired from the oblong region between points *A* and *B*. Parallel selections denoted $a-e$ refer to the areas with different LEED patterns observed (see Fig. 2). (b) Integrated cross-section intensity obtained from the oblong region between points *A* and *B* in (a). The width of the transition region between the clean Si(111)-(7×7) surface and 1 ML Au is approximately 10 μm. The slope of the curve between 0 and about 9 μm is an artefact due to background modulation.

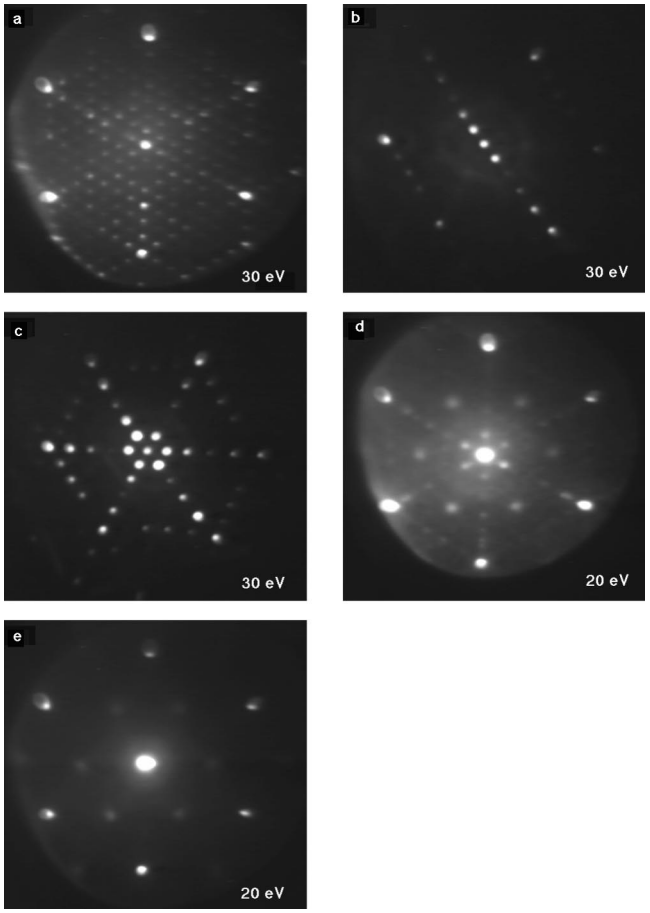

FIG. 2. μ-spot LEED patterns of selected areas a–e in Fig. 1(a). The energies of the primary electron beam are given in the lower right-hand corners.

limit of the various reconstructions, we utilized the LEED mode of the SPELEEM to obtain locally resolved structural information from the transition zone. By selection of the smallest illumination aperture available, a detection area of only 1 μm^2 was achieved (μ-spot LEED). Representative diffraction patterns are shown in Fig. 2 corresponding to the regions a to e indicated in Fig. 1(a). The sequence demonstrates that starting with the (7×7) LEED pattern on the uncovered Si(111) part, regions b and c display the lowest coverage (5×1) reconstruction. Figure 2(b) shows one domain while the full set of the three possible symmetry domains is seen in Fig. 2(c). Region d presents the transition from (5×1) to the $(\sqrt{3}\times\sqrt{3})R30°$ structure, evident from the superposition of both LEED patterns in Fig. 2(d). The $\beta\sqrt{3}$ pattern characteristic of the monolayer gold coverage is found in region e, although the ordering is not so distinct as in the other regions, as is apparent from the more diffuse diffraction spots. Summarizing, the border region of the initial state represents a well-ordered transition zone where the gold concentration decreases continuously from 1 ML Au layer to the clean reconstructed Si(111).

To determine the onset of diffusion we monitored the PEEM image of the border region in real time while increasing the sample temperature very slowly to ensure a uniform temperature over the whole sample. The transition zone of the initial state developed a sharp steplike shape, until at $\approx$970 K this boundary started to spread into the uncovered

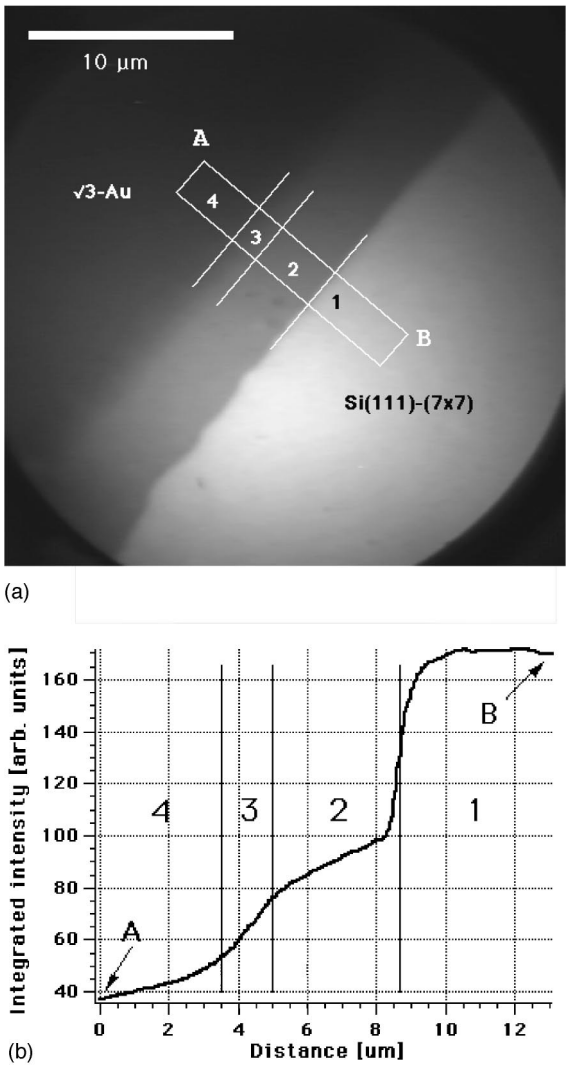

FIG. 3. (a) Ordered Au regions observed in the early stages of diffusion. The image was acquired in the PEEM mode. See Fig. 4 for the LEED patterns of the areas denoted as 1–4. (b) Integrated cross-sectional intensity obtained from the oblong region between points A and B in (a).

region. An early stage of the evolution is shown in the PEEM image of Fig. 3(a) where the development has been frozen by quenching the sample to room temperature. The difference from the border distribution in Fig. 1(a) is evident. Immediately commencing at the sharp intensity drop at the interface with the Si(111)-(7×7) surface [region 1 in Fig. 3(a)], an area with slowly decreasing intensity (region 2) has evolved followed by a transition part (region 3), which merges into the darkest part of the image. The complex structure of the boundary is more obvious from the intensity profile in Fig. 3(b), illustrating both the sharp edge and the plateau-like distribution of the foremost zone. Structural information of the areas indicated by the numbers 1 to 4 in Figs. 3(a) and 3(b) was again obtained by applying μ-spot LEED with the corresponding patterns given in Fig. 4. Regions 2 and 4 uniformly showed the (5×1) and $(\sqrt{3}\times\sqrt{3})R30°$ superstructures, respectively. The latter exhibited substantially sharper LEED spots, indicating a better ordering of the layer [compare Figs. 2(d) and 2(e)]. The transient zone between these two superstructures is characterized

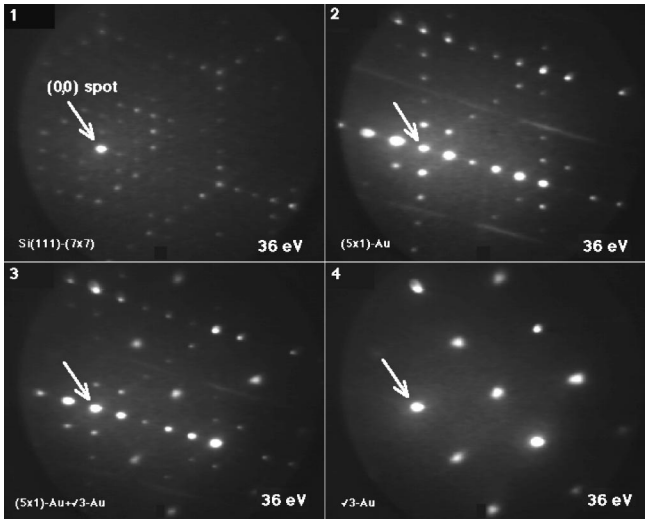

FIG. 4. μ-spot LEED patterns of the selected areas 1–4 in Fig. 3(a). The (0,0) spot is denoted by the white arrows. All the structures are well ordered. The energies of the primary electron beam are given in the lower right-hand corners.

by the superposition of the patterns of both adjacent regions. If the diffusion process proceeds further, the transient zone corresponding to region 3 in Fig. 3(a) moves much slower than the interface between the Au covered region and Si(111)-(7×7). The edge of the (5×1) ordered area maintained its shape.

A more direct determination of the concentration distribution of Au (and as complementary information of Si) across the border can be obtained by using the XPEEM imaging mode of the SPELEEM.[12] By excitation of characteristic photoemission lines of the element to be monitored with elevated photon energies and application of an energy filter one can image the substrate with these photoelectrons, i.e., with chemical contrast. Thus, in general, the brightness in XPEEM is proportional to the concentration. Figure 5 shows the border region that corresponds roughly to the PEEM image in Fig. 3(a) but is imaged in the XPEEM mode illustrating the Si (left image, Si $2p$ core level states) and the Au (right image, Au $4f_{7/2}$ core level states) surface concentration map. The Si(7×7)/Au(5×1) interface is evident in both maps by the sharp transition from the bright part to the dark region. Even if the intensity in the XPEEM mode is substantially weaker than in the PEEM mode, on closer inspection the characteristic plateau-like region of the (5×1) reconstruction is discernible (see the arrows in Fig. 5). Since the Au $4f_{7/2}$ image is directly related to the Au concentration, SPELEEM with the energy filter tuned to the Au $4f_{7/2}$ photoemission line was used to monitor the spreading of the Au layer. The resulting sequence of images is displayed in Fig. 6(a) for a substrate temperature of 985 K and a time interval of 30 s between consecutive images.

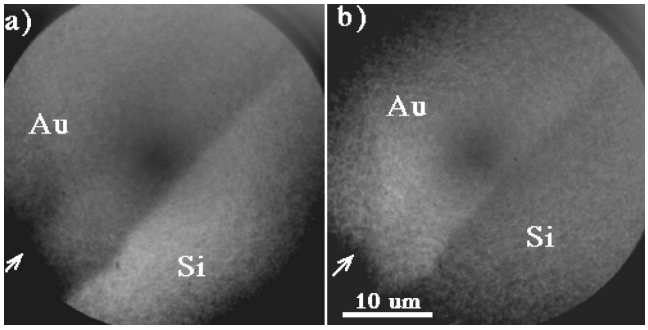

FIG. 5. XPEEM images of the border region. The energy filter of SPELEEM was tuned to (a) the Si $2p$ and (b) the Au $4f_{7/2}$ photoemission lines.

Normalized intensity profiles obtained from the sequence of XPEEM images [taken in the region indicated in image 1 of Fig. 6(a)] are plotted in Fig. 6(b). Since the electron yield of the channel plates was not homogeneous (see the intensified patch in all the images), the following normalization procedure has been applied. The background of the first profile was fitted with a second-order polynomial (not shown here) and all profiles were divided by this parabolic curve. In addition, to estimate reliably the border position in spite of the noise level, each profile was approximated with 3 straight lines as indicated in the inset of Fig. 6(b). The respective intersections yield two points: the highest (A) and the lowest (B) Au concentration. These two points are considered to define the diffusion zone, i.e., the transition zone between the gold-covered regions and the clean Si(111)-(7×7) surface. The positions of the points A and B are plotted in Fig. 7 as a function of time with the border positions of the first profile serving as time zero. It is evident that the propagation velocity of the border diminishes with time. The separation between the two characteristic points (A and B), however, increases. To summarize, the movement of the diffusion zone can be described as a combination of two effects: (i) the evolution of a characteristic S-shape concentration profile which is (ii) moved as a whole in the direction of lower concentration. Unfortunately, we were not able to perform an intensity versus concentration calibration. Therefore, the concentration dependence of the diffusion coefficient cannot be extracted from the data, e.g., by applying a Boltzmann-Matano analysis. On the other hand, a spatially averaged diffusion coefficient is determined in the following.

In order to trace the expansion of the (5×1)-reconstructed area and, in particular, the steplike border line in more detail, we operated the SPELEEM in the MEM imaging mode. Since in MEM incoming electrons have energies just below the work function threshold, they are reflected at the repulsive potential of the substrate and the contrast of a MEM image arises from the corrugation of the surface potential. The MEM mode is thus ideally suited to detect inhomogeneities on a surface, such as defects or potential steps, with high sensitivity and resolution. After preparation of a new step profile, diffusion was activated until the (5×1) area had sufficiently developed to be clearly separated from the $\sqrt{3}$-Au area (4 min at $\approx$970 K). After cooling the sample below the diffusion threshold, the microscope was switched to MEM mode and the first two images of Fig. 8 obtained at $\approx$850 K. Both the (5×1)-Au and the Si(111)-(7×7) areas appear absolutely homogeneous (apart from the marked defect), indicating a well-developed ordering in the respective parts. Diffusion resumed after heating the sample again to $\approx$970 K. The onset of this later diffusion stage is captured in image 3 and proceeds in the sequence from image 4 to 12 acquired every 30 s. The indicated defect did not pin the diffusion front but only delayed its progress.

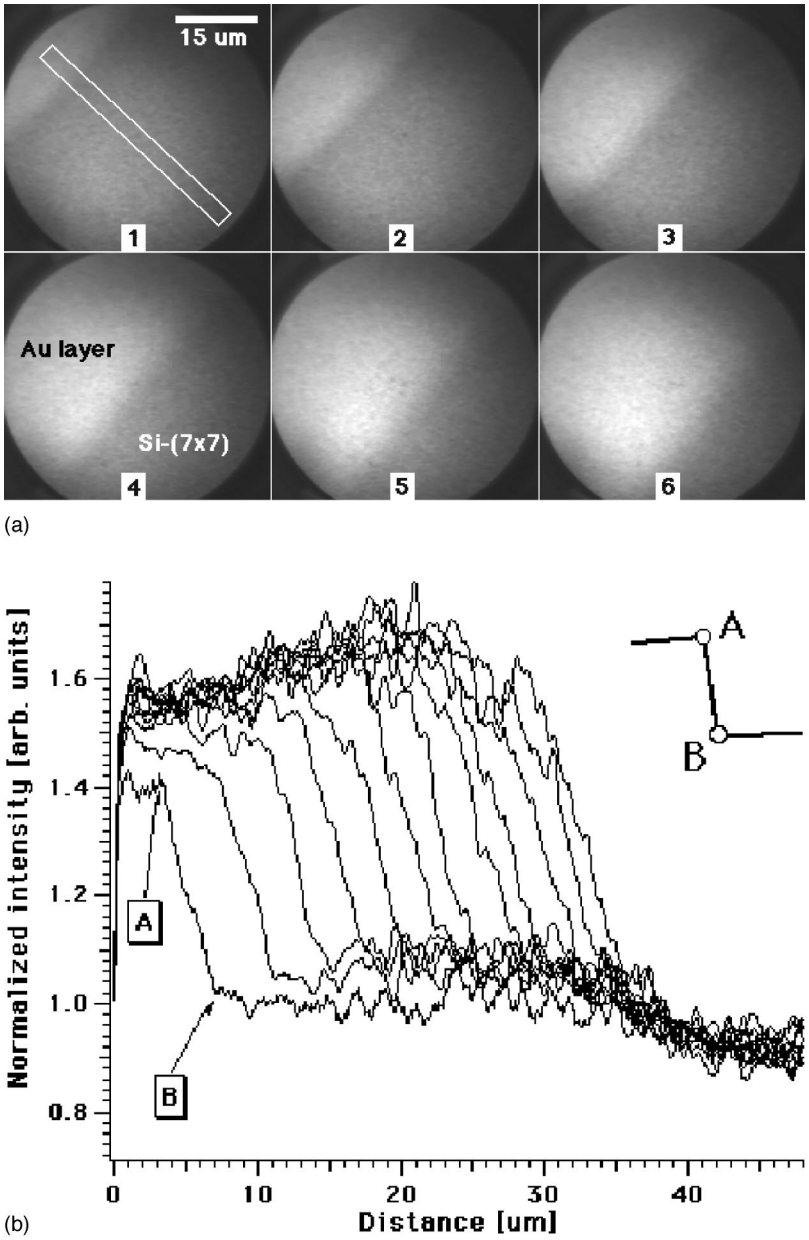

FIG. 6. (a) Selected sequence of images in XPEEM mode taken during diffusion. Photon energy $h\nu = 150$ eV, kinetic energy 82 eV, Au $4f_{7/2}$ core level. The field of view is 50 μm in each image, and the time interval between images is 30 s. The sample temperature for all images was 985 K. (b) Intensity profiles determined from the sequence of XPEEM images. Profiles were taken along the line indicated in (a). Each profile was fitted with three straight lines (see the upper right-hand corner of the figure). The cross sections of the lines define the point *A* (the highest Au concentration) and the point *B* (the lowest Au concentration).

Two aspects of the sequence in Fig. 8 are noticeable. First, only the moving boundary exhibits a bright fringe (see images 3–12) while for the frozen state (images 1 and 2) the edge shows a rich structure but is not highlighted. Figure 9 shows a magnified picture of the tenth image in Fig. 8 showing more distinctly the bright patches at the edge. Initially they form islands, thus giving rise to inhomogeneities of the potential surface that are imaged in MEM as bright blotches. Later these islands coalesce and merge into the (5×1) region. Second, as already evident from image 1 of Fig. 8, the steplike border does not conserve the initially straight-line form but develops a regular shape consisting of joint line segments. The angle between the lines turned out to be always $135° \pm 10°$ (see Fig. 9), whereby the estimated error is mainly due to image distortions originating from the magnetic lens systems. Unfortunately, the existing structure models of the (5×1)-Au reconstruction[9,10] that would favor multiples of 30° do not allow easy correspondence of this angle with the preferred directions of the elementary lattice cells. In a recent STM study of the growth of the (5×1)-Au reconstruction[10,15] it has been observed that at the border of a (5×1) domain, which appears in STM as a row structure along a high symmetry direction of the Si(111) surface, additional rows grow along the existing ones. In some cases bunches of such new rows appear, growing in a concerted way and forming a dynamic border line at their ends, which is inclined with respect to the row direction. This orientation might be at the angle observed here but the scale gap between the atomic scale of the STM (only up to seven rows in a bunch) and our mesoscopic resolution (line segments of several μm length) prevents any further correlation. In addition, it is not possible to determine precisely the real space azimuthal orientation of the substrate from the LEED pattern since the magnetic lenses in the electron optical path of the SPELEEM rotate the diffraction pattern.

The sequence in Fig. 8 shows the zone movement as a function of time through the area indicated in Fig. 9. The position of the border in image 3 in Fig. 8 was taken as the starting configuration, i.e., $x = 0$, for the graph in Fig. 10. The zone movement is evidently almost linear in time.

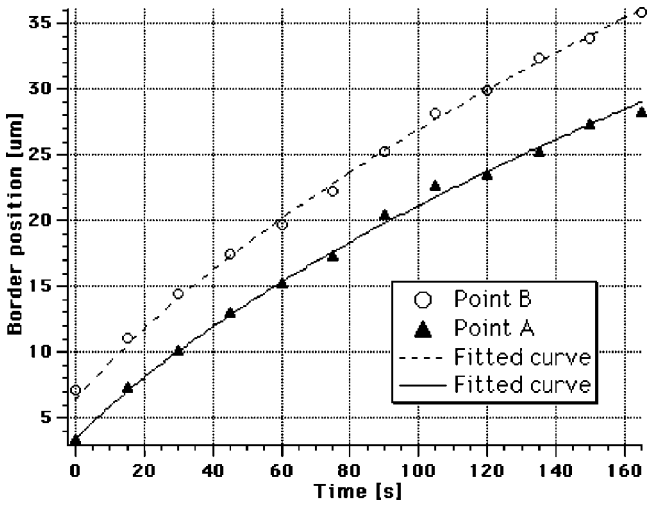

FIG. 7. Border position as a function of time. The two sets of points correspond to the points *A* and *B* in Fig. 6(b).

IV. DISCUSSION

From the above results it is obvious that the system Au on Si(111)-(7×7) is far from being a simple diffusion system described by a constant diffusion coefficient, which would produce the typical sigmoidal concentration profile (see Ref. 16). The development of the rather complex structure in the diffusion front [see Figs. 3(a) and 3(b)] clearly indicates that the diffusion coefficient is strongly coverage dependent passing through maximum and minimum values. As a rule of thumb, steep concentration increases are connected to low values while the flat parts are due to a local maximum of the diffusion coefficient, which is particularly pronounced for the extended (5×1) regions at later stages of the diffusion (see Fig. 8). Similar findings have been presented for some metal on metal diffusion studies but mainly for multilayer diffusion.[4] For the system presented here the rich structure in the $D(\Theta)$ dependence in the submonolayer regime is certainly caused by the formation of the various reconstructed phases.

If we describe the results as nearly as possible in terms of classical diffusion theory with a coverage dependent diffusion coefficient (see Ref. 16) the initial stage is best approximated as a one-dimensional problem with a semi-infinite step distribution. For a constant diffusion coefficient the initial concentration c_0 would expand into the initially zero concentration region according to

$$c(x,t)=\frac{1}{2}c_0\,\mathrm{erfc}\left(\frac{x}{\sqrt{4Dt}}\right). \tag{1}$$

In consequence, if a particular concentration level can be identified and its position monitored during diffusion, the movement follows $x\approx\sqrt{Dt}$. In the system here such a tagging occurs dynamically through the formation of the borders visible in Fig. 3(a). Thus, the SPELEEM images presented demonstrate the outward spread of the Au atoms forming the $\sqrt{3}$ and the (5×1) regions while being released from the virtually infinite source of the 1 ML area covering half of the sample. The XPEEM images in Fig. 6(a) obtained at an early diffusion stage show essentially the combined transition zone limited by both the edges to the $\sqrt{3}$ and to the (5×1) reconstruction phases, thus defining the points *A* and *B* as determined in the analysis of the concentration profiles in Fig. 6(b). Both sets of data points in Fig. 7 follow almost perfectly the $\sqrt{Dt}$ behavior as evident from the fit curve also shown in Fig. 7. The fitting function used was

$$x_{A,B}=x_0+\sqrt{2D_{A,B}(t+t_0)} \tag{2}$$

with x_0 and t_0 acting as free fit parameters because neither the initial border position nor the effective starting time can be directly determined from the time sequence of the XPEEM images. The resulting values of $x_0=-15$ μm and $t_0=35$ s are reasonable in view of the experimental preliminaries of sample adjustment and temperature stability. The calculated diffusion coefficients are $D_A=4.8\times10^{-8}$ cm^2 s^{-1} and $D_B=6.5\times10^{-8}$ cm^2 s^{-1}. It can be concluded that although a phase transition occurs in the dif-

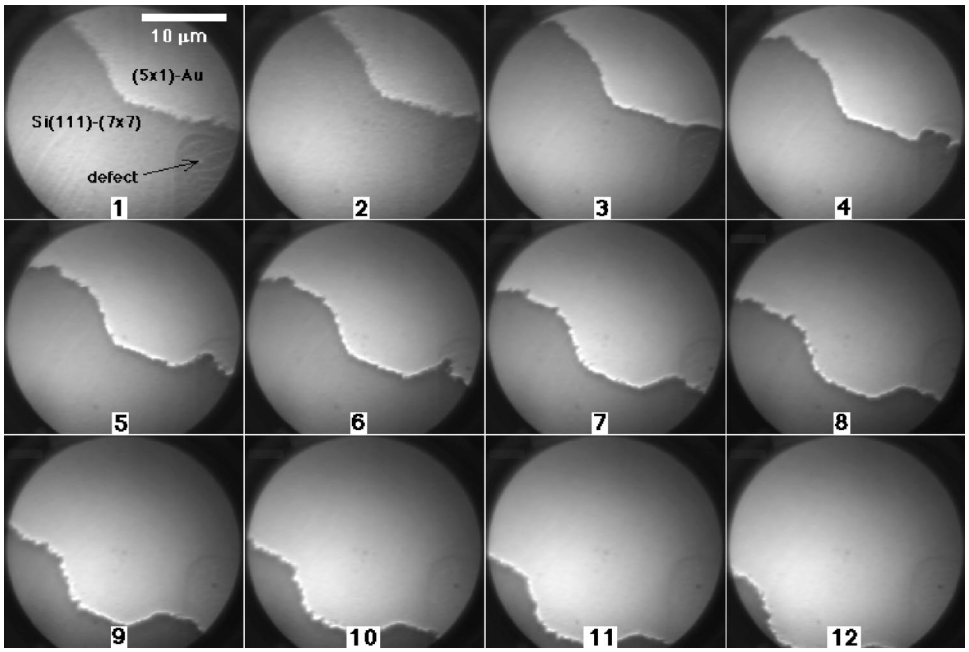

FIG. 8. Selected sequence of images in MEM mode taken during diffusion. The field of view is 27 μm in each image, and the time interval between neighboring images is 30 s. The sample temperature in the first image was 850 K, in the second image it was 910 K, and for all following images it was 970 K. Diffusion starts in the third image. The defect in the first image was chosen as an immobile marker.

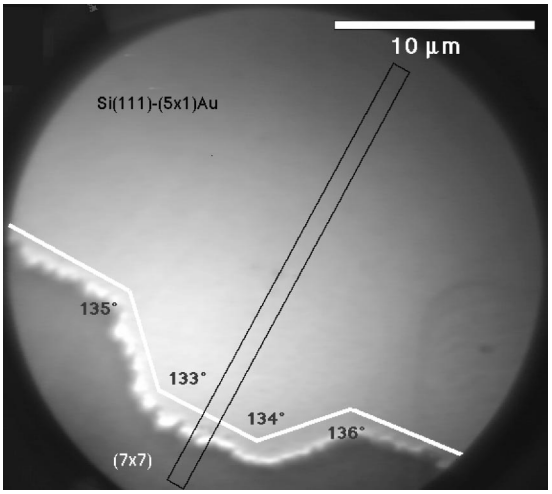

FIG. 9. Detail of the tenth image in Fig. 8, which shows a tendency to self-organize and retain a regular shape during diffusion.

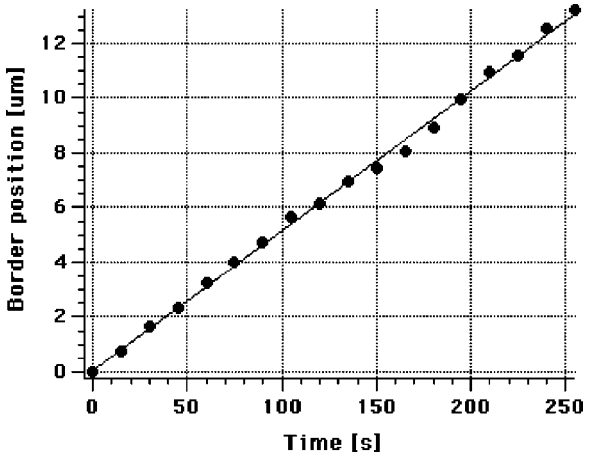

FIG. 10. Border position as a function of time measured along the region indicated in Fig. 9. The fitted curve is a straight line.

fusion front, the outward particle flux is essentially governed by the concentration gradient since the movement of both borders obeys the classical diffusion equation.

Even though the difference of the two diffusion coefficients seems to be insignificant in view of the experimental uncertainties, the data in Fig. 7 clearly demonstrate that points *A* and *B* move with different velocity, leading to an increasing separation. This behavior is in strong contrast to the constant velocity of the (5×1)Au/Si(7×7) edge movement documented in MEM measurements at later stages of diffusion (see Fig. 10). This is typical for stationary or quasistationary conditions where a particle flux is constant. Noting that the diffusion coefficient exhibits a strong maximum at the coverage corresponding to the (5×1) reconstruction, the evolution of the (5×1) terrace can be treated to a good approximation as a diffusion problem with the boundary conditions of fixed concentrations (or equally well-fixed particle fluxes at the boundaries). In our system, these concentrations correspond to $\sqrt{3}$-Au and (5×1)-Au bordering on the Si(111)-(7×7) region. For the situation in Fig. 8 the size of the (5×1) terrace is certainly large enough so that the concentration profile over the terrace is essentially linear, i.e., the gradient and thus the particle flux are constant. In a microscopic picture, this kind of behavior is very often described as the unrolling carpet mechanism.[17] A particle that is released from a high concentration border [here the border between the (5×1) and the $\sqrt{3}$ zones] diffuses over an almost constant concentration terrace until it reaches the edge of a low concentration region [here the end of the (5×1)-Au plateau], thereby extending the terrace region. Such a model requires that the additional particle on top of the terrace experiences a smaller diffusion barrier than the particles constituting the terrace. In our system the fifth Au atom in the (5×1) unit cell[9,10] can serve as a suitable candidate because for the structure model proposed in the literature, the unit cell consists of either 4 or 5 atoms, giving rise to coverages of $\Theta=0.4$ ML or $\Theta=0.5$ ML, respectively. The fifth atom in the unit cell is observed to become highly mobile above 450 K.[10]

A reasonable estimate of the diffusion coefficient for Au atoms on Si(111)-(7×7) at a coverage from 0.4 ML up to 0.66 ML can be deduced from the front velocity given in Fig. 10. Evaluating the particle flux at the (5×1)Au/Si(7×7) border yields $J=1.8\times10^{9}$ cm^{-1} s^{-1}. Assuming that (a) the Au concentration varies over the (5×1) terrace from $\Theta=0.66$ ML at the $\sqrt{3}$ border ($c_1=5.28\times10^{14}$ cm^{-2}) to $\Theta=0.4$ ML at the opposite end ($c_2=3.13\times10^{14}$ cm^{-2}) and (b) the (5×1) terrace is about $\Delta x_{5\times1}\approx50$ μm wide, the averaged diffusion coefficient from

$$D_C=\frac{J\Delta x}{c_1-c_2} \tag{3}$$

is $D_C=4.2\times10^{-8}$ cm^2 s^{-1}. Despite this being a simple approximation, it yields good agreement with D_A and D_B found above by a fitting procedure. Summarizing, the average diffusion coefficient $D_{7\times7}$ for Au particles on Si(111)-(7×7) in a coverage interval from 0.4 ML to 0.66 ML equals $D_{7\times7}=5.2\times10^{-8}$ cm^2 s^{-1}. First, we point out that $D_{7\times7}$ is related to the stated coverage interval since diffusion on the otherwise intact Si(7×7) surface could result in quite a different value. Second, though D_A, D_B, and D_C were obtained at slightly different temperatures (985 K and 970 K, respectively), we consider them well comparable: Apart from experimental uncertanties in temperature reading, diffusion coefficients at these two temperatures would differ by $\approx17\%$, using the activation energy of diffusion $E_d=1$ eV.

Similarly within this simple model the lower limit of the diffusion coefficient $D_{5\times1}$ for highly mobile Au atoms moving on the (5×1)-Au plateau can be estimated. We suppose that in the vicinity of the border with $\sqrt{3}$-Au the concentration corresponds to the saturated (5×1) phase ($\Theta=0.5$ ML, i.e., $c_1=3.91\times10^{14}$ cm^{-2}) and the other end of the plateau possesses the lowest possible concentration ($\Theta=0.4$ ML, i.e., $c_2=3.13\times10^{14}$ cm^{-2}). Using the above equation with $\Delta x_{5\times1}\approx50$ μm we obtained $D_{5\times1}=1.2\times10^{-7}$ cm^2 s^{-1}, i.e., more than twice the magnitude of $D_{7\times7}$.

In agreement with the diffusion mechanism proposed above particle fluxes on the plateau and in the region between the points *A* and *B* [Figs. 6(a) and 7] must be equal due to the conservation of Au particles. Generally in the case of isotropic diffusion, flux is given as the product of a diffu-

sion coefficient and a concentration gradient.[16] Assuming that the two fluxes are equal, we arrive at a simple equation for the diffusion coefficient on (5×1)-Au evaluated independently from above procedure:

$$D_{5\times1}=D_{7\times7}\frac{\mathrm{grad}(c_1)}{\mathrm{grad}(c_{5\times1})}, \tag{4}$$

where $\mathrm{grad}(c_{5\times1})$ and $\mathrm{grad}(c_1)$ describe a concentration gradient on the plateau and between the points *A* and *B* in Fig. 7, respectively. Applying typical values (for $\Delta x_{AB}\approx4$ μm see Fig. 7 and $\Delta x_{5\times1}\approx50$ μm), we derive for the lower limit of $D_{5\times1}\cong50D_{7\times7}$, i.e., $D_{5\times1}$ is considerably higher again.

The present values of the diffusion coefficient are in rough agreement with the value given by Nesterenko *et al.*[18] based on measurements at low spatial resolution. Due to the lack of recent experiments dealing with metal diffusion (in the submonolayer coverage range) on Si(111)-(7×7) we cannot compare directly our values of *D* with experimental data. However, the diffusion coefficient is a quantity that represents a relationship between the transferred mass (the flux) during a measured time interval and the concentration gradient. If both these quantities in some experiment are comparable to the present values, then the diffusion coefficient should also lie within a certain range regardless of diffusion temperature. Under these considerations we conclude that $D\approx10^{-8}$ cm^2 s^{-1} is not unreasonable.[1,4]

As an alternative mechanism for an extension of the (5×1) reconstruction with constant velocity, we considered a chemical reaction with a moving reaction front. Supposing that the formation of (5×1) reconstruction is connected with a reaction between the Si and the Au atoms, the reaction rate is proportional to the concentration of both species: $r\propto[\mathrm{Au}][\mathrm{Si}]$. The number of Si atoms at the reaction front is obviously constant, as is the number of Au atoms determined by the diffusion flux. In the stationary stage of the process, the reaction rate will be constant as well and the reaction front will move to the area with higher Si atom concentration because the mobility of Au atoms is higher.

V. CONCLUSIONS

Measurements of Au/Si(111) surface diffusion at submonolayer coverages have been carried out using chemical contrast imaging. A direct quantitative evaluation of the (5×1)-Au ordered phase evolving on Si(111)-(7×7) has been performed, applying a combination of different microscopic and spectroscopic modes. The diffusion of Au atoms has been interpreted in terms of the ''unrolling carpet'' mechanism. Two diffusion coefficients were estimated at a temperature of about 985 K: (1) $D_{7\times7}=5.2\times10^{-8}$ cm^2 s^{-1} as the averaged diffusion coefficient for Au diffusion on a clean Si(111)-(7×7) surface in a concentration range from 0.4 ML up to 0.66 ML and (2) $D_{5\times1}=1.2\times10^{-7}$ cm^2 s^{-1} as the lower limit for the diffusion of Au atoms on the Si(111)-(5×1)-Au ordered phase. In order to obtain a real concentration-dependent diffusion coefficient from a Boltzmann-Matano analysis, further measurements are desirable.

ACKNOWLEDGMENTS

The investigation was supported by the Grant Agency of the Czech Academy of Sciences (Grant No. A1010718), the Grant Agency of the Czech Republic (Grant No. 202/99/P001), and by the Deutsche Forschungsgemeinschaft through SFB 290. Th. Schmidt and B. Ressel acknowledge support under EU contracts ERB FMBI-CT 96-1749 and ERBIC 15 CT97 0700, respectively. The SPELEEM instrument was supported by the Deutsche Forschungsgemeinschaft, the Bundesministerium für Bildung und Forschung, and the VW-Stiftung.

*Corresponding author FAX: +420 2 3123184. Electronic address: slezak@fzu.cz

[1] M. Snabl, M. Ondrejcek, V. Chab, Z. Chvoj, W. Stenzel, H. Conrad, and A. M. Bradshaw, J. Chem. Phys. **108**, 4212 (1998).
[2] M. Ondrejcek, V. Chab, W. Stenzel, M. Snabl, H. Conrad, and A. M. Bradshaw, Surf. Sci. **331-333**, 764 (1995).
[3] A. G. Naumovets, M. V. Palyi, and Yu. S. Vedula, Phys. Rev. Lett. **71**, 105 (1993).
[4] A. G. Naumovets and Yu. S. Vedula, Surf. Sci. Rep. **4**, 365 (1985), and references therein.
[5] C. Cohen, Y. Girard, P. Leroux-Hugon, A. L'Hoir, J. Moulin, and D. Schmaus, Europhys. Lett. **24**, 767 (1993).
[6] H. Yasunaga, Surf. Sci. **242**, 171 (1991).
[7] A. Yamanaka and K. Yagi, Surf. Sci. **242**, 181 (1991).
[8] W. Swiech, E. Bauer, and M. Mundschau, Surf. Sci. **253**, 283 (1991).
[9] R. Plass and L. D. Marks, Surf. Sci. **380**, 497 (1997).
[10] T. Hasegawa and S. Hosoki, Phys. Rev. B **54**, 10 300 (1996).
[11] S. Ino, in *RHEED and Reflection Electron Imaging of Surfaces*, edited by P. K. Larsen and P. J. Dobson (Plenum, New York, 1998), p. 3.
[12] Th. Schmidt, S. Heun, J. Slezak, J. Diaz, K. C. Prince, G. Lilienkamp, and E. Bauer, Surf. Rev. Lett. **5**, 1247 (1998).
[13] P. A. Bennett and M. B. Webb, Surf. Sci. **104**, 74 (1981).
[14] A. Kolmakov, M. Bertolo, S. Fontana, S. Günther, J. Kovac, M. Marsi, and M. Kiskinova, Surf. Sci. **377-379**, 969 (1997).
[15] T. Hasegawa, S. Hosoki, and K. Yagi, Surf. Sci. **355**, L295 (1996).
[16] J. Crank, *The Mathematics of Diffusion*, 2nd ed. (Oxford University Press, London, 1975).
[17] M. C. Tringides, *Surface Diffusion* (Plenum Press, New York, 1997), Vol. 360, p. 494.
[18] B. A. Nesterenko, V. A. Zrazhevskii, and V. T. Rozumnyuk, Fiz. Tverd. Tela (Leningrad) **19**, 3284 (1977) [Sov. Phys. Solid State **19**, 1919 (1977)].